Emergence of ionization balance plasma in confinement region with the complete divertor detachment

Motoshi GOTO, Shigeru MORITA

National Institute for Fusion Science, Toki 509-5292, Japan

October 29, 2007

A spectroscopic measurement is made for the plasma in the rotating radiation belt accompanying the complete divertor detachment which is recently realized in the Large Helical Device (LHD) [J. Miyazawa, et al., Nucl. Fusion **46**, 532 (2006)]. The Balmer series lines of neutral hydrogen are clearly observed. The population distribution over the exited levels is determined from the Balmer series line intensities and is compared with the result of the collisional-radiative model calculation to determine the electron temperature T_e and density n_e. No reasonable pair of T_e and n_e is found when either the ionizing plasma or the recombining plasma is assumed. A good fitting is obtained under an assumption of the ionization balance plasma with $T_e = 1.8\,\mathrm{eV}$ and $n_e = 2 \times 10^{20}\,\mathrm{m}^{-3}$. The mechanism to sustain such a low temperature plasma inside the high temperature confinement region is unclear.

Keywords: radiation belt, spectroscopy, ionization balance plasma, Stark broadening

1 Introduction

In the study of magnetic confined fusion plasma the reduction of heat flux onto the divertor plate is an important issue. A possible solution of this problem is to induce the detached plasma in the divertor region through intentional radiation loss. For this purpose the impurity gas puffing has been attempted in various devices [1–5].

In the Large Helical Device (LHD) the complete detachment of the divertor plasma has been obtained with strong gas puff of hydrogen into the divertor region. A salient feature of the obtained plasma in LHD is that it is accompanied by emergence of a luminous radiation belt in the boundary region which has a helical structure and surrounds the core plasma. Furthermore, the radiation belt looks poloidally rotate with a frequency of, for example, 15 Hz.

Though the conditions of the discharge to obtain such a detached plasma have been investigated in detail [6], the plasma state in the radiation belt itself is still unclear. Our interest is the plasma state in the strong radiation region and its relevance to the occurrence of plasma detachment. This paper introduces our attempt to determine the plasma state and parameters, such as the electron temperature T_e and the electron density n_e, in the radiation belt from the measured spectra in the visible wavelength range.

2 Experiment

LHD is a heliotron type fusion experimental device of magnetic confinement. It forms a steady-state structure of magnetic field with a set of super-conducting coils. The plasma has an elliptical poloidal cross section and it rotates with a toroidal period number of five. The major and averaged minor radii of the last closed flux surface are 3.5 m–4.2 m and 0.6 m, respectively.

We use an optical fiber having the diameter of 100 μm to observe the light emitted from the plasma. One end of the optical fiber is placed at the observation port, and the field of view of the optical fiber is collimated with a lens so as to have a cylindrical shape with the diameter of roughly 30 mm in the plasma. The optical axis passes through the plasma center as shown in Fig. 1. The other end of the optical fiber is located at the entrance of a spectrometer. The spectrometer has a focal length of 50 cm and is equipped with three gratings of 100, 1800, and 3600 grooves mm^{-1}, respectively. The spectrum is recorded with a CCD (charge coupled device) detector. The maximum sampling rate is 200 spectra s^{-1}. The sensitivity of the whole observation system has been absolutely calibrated with a tungsten lamp.

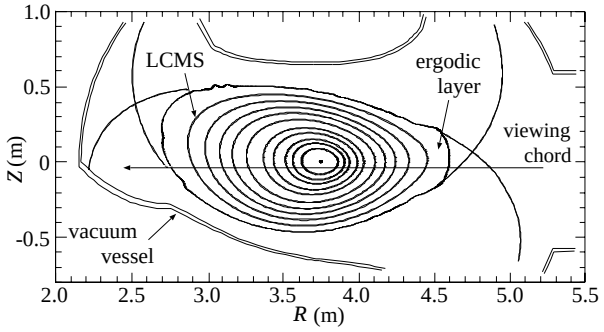

Fig. 1 Cross section of the vacuum vessel and the plasma for our observation. The major radius of the vacuum vessel center is 3.9 m. The plasma is observed with a single line-of-sight shown with the arrow.

author's e-mail: goto@nifs.ac.jp

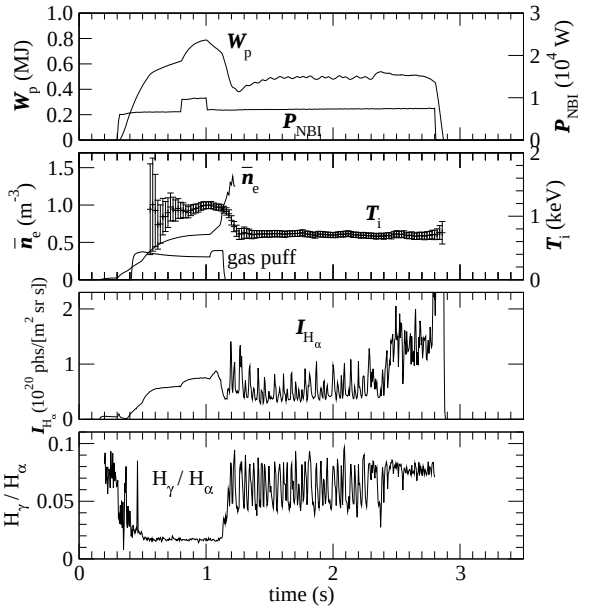

Fig. 2 Temporal development of the discharge for the present analysis. The measurement of the line-averaged electron density, $\bar{n}_e$ with the interferometer is limited until $t = 1.2$ s due to the fringe jump problem. The ion temperature, T_i, is determined from the Doppler width of a helium-like argon ion line.

Figure 2 shows the temporal behavior of a discharge for which the complete detachment has been obtained. The present experiment employs the magnetic configuration of $R_{ax} = 3.65$ m and $B_{ax} = 2.712$ T, where R_{ax} and B_{ax} are the magnetic axis radius and the magnetic field strength on the magnetic axis, respectively.

The plasma is sustained with three neutral beams ($\sim$ 7 MW). The line-averaged electron density $\bar{n}_e$, which is measured with the interferometer, is feedback-controlled with the gas puffing rate until $t = 1$ s. At $t = 1$ s a short pulse massive gas puff (~ 0.1 s and ~ 200 Pa m^3 s^1) is given and $\bar{n}_e$ suddenly increases. The $\bar{n}_e$ measurement is unavailable after $t = 1.2$ s due to fringe jump problem.

After such an abrupt change in $\bar{n}_e$, the stored energy W_p and the central ion temperature T_i, which is determined from the Doppler broadening of the heliumlike argon resonance line, are kept almost constant. During this stationary time period the particle flux onto the divertor plate, which is measured with Langmuir probes, is found decreased and the plasma detachment is suggested [7]. Simultaneously, the measurement with an absolute extreme ultra violet photodiode (AXUVD) camera [8] suggests the emergence of a rotating radiation belt [7].

Spectra of the emitted light from the plasma are measured with the 100 grooves mm^{-1} grating out of three. The wavelength range of 300 nm to 700 nm is simultaneously observed. Each emission line is fitted with a Gaussian function and the corresponding intensity is derived as the area of the line profile. The temporal variations of the Balmer α (656.3 nm) line intensity and the intensity ratio of the Balmer γ (434.0 nm) to α lines are shown in Fig. 2.

It is readily noticed that the Balmer α line intensity oscillates with a frequency of approximately 30 Hz which is twice the frequency of the radiation belt rotation derived from the AXUVD measurement. This is understandable because in a cycle of the radiation belt rotation the line intensity should take the maximum twice when the radiation region crosses the line-of-sight at the near side and the far side of the plasma edge. The ratio of the Balmer γ and Balmer α lines is also found oscillating with the same frequency. This result suggests that the plasma states inside and outside the radiation belt are considerably different.

3 Collisional-radiative model

We use the collisional-radiative (CR) model code [10] for the analysis of the obtained spectra. The CR model is based on the rate equations concerning the excited level populations. The time derivative of the population of a level p, $n(p)$, is expressed as

$$\frac{\mathrm{d}}{\mathrm{d}t} n(p) = \Gamma_{in}(p) - \Gamma_{out}(p), \tag{1}$$

where $\Gamma_{in}(p)$ and $\Gamma_{out}(p)$ stand for the population flows into the level p and out of the level p, respectively. These population flows are explicitly written with various elementary atomic processes as

$$\begin{aligned}\Gamma_{in}(p) &= \sum_{q>p} A(q,p)n(q) + \sum_{q<p} C(q,p)n_e n(q) \\ &\quad + \sum_{q>p} F(q,p)n_e n(q) + \beta(p)n_e n_i + \alpha(p)n_e^2 n_i \\ &= \sum_{q<p} C(q,p)n_e n(q) \\ &\quad + \sum_{q>p} \{F(q,p)n_e + A(q,p)\}\, n(q) \\ &\quad + \{\beta(p) + \alpha(p)n_e\}\, n_e n_i, \end{aligned} \tag{2}$$

and

$$\begin{aligned}\Gamma_{out}(p) &= S(p)n_e n(p) + \sum_{q>p} C(p,q)n_e n(p) \\ &\quad + \sum_{q<p} F(p,q)n_e n(p) + \sum_{q<p} A(p,q)n(p) \\ &= \Bigg[S(p)n_e + \sum_{q>p} C(p,q)n_e \\ &\quad + \sum_{q<p} \{F(p,q)n_e + A(p,q)\} \Bigg] n(p), \end{aligned} \tag{3}$$

respectively, where $S(p)$, $\alpha(p)$, and $\beta(p)$ are the rate coefficients for the electron impact ionization, three-body recombination, and radiative recombination, respectively, and $C(p,q)$ and $F(p,q)$ are the excitation and deexcitation rate coefficients, respectively, due to electron impacts from

level p to level q. The expression $\sum_{q>p}$ means that the summation is conducted over the excited levels located higher than p.

The relaxation time of the excited level populations is generally so short that the left-hand-side of Eq. (1) is assumed to be zero except for the ground state and the ion. In this case, a collection of Eq. (1) for the all excited levels is regarded as a set of coupled linear equations which is solved readily. As the solution of the coupled equations $n(p)$ is found to be expressed as a linear combination of two terms which are proportional to the ground state density $n(1)$ and ion density n_i, respectively, like

$$n(p) = R_0(p) n_\mathrm{e} n_\mathrm{i} + R_1(p) n_\mathrm{e} n(1), \tag{4}$$

where the first and the second terms are called the recombining plasma component and the ionizing plasma component, respectively, and $R_0(p)$ and $R_1(p)$, which are functions of T_e and n_e, are called the population coefficients.

Equation (1) for the ground state atom and ion can be rewritten in the form as

$$\frac{\mathrm{d}}{\mathrm{d}t} n(1) = -\frac{\mathrm{d}}{\mathrm{d}t} n_\mathrm{i} = -S_\mathrm{CR} n_\mathrm{e} n(1) + \alpha_\mathrm{CR} n_\mathrm{e} n_\mathrm{i}, \tag{5}$$

where S_CR and α_CR are composed from the obtained population coefficients and correspond to the effective ionization and recombination rate coefficients, respectively.

4 Results

Figure 3 shows the spectrum when the Balmer α line intensity takes maximum during the oscillation phase. This

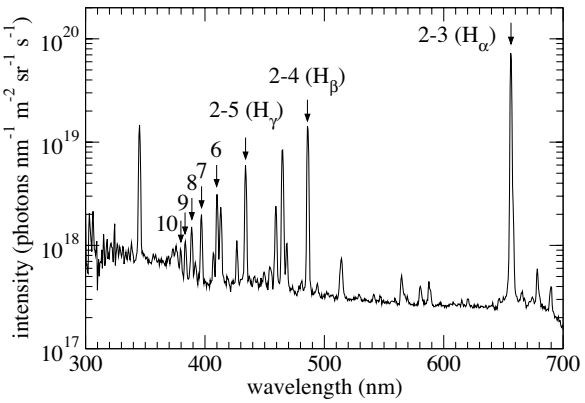

Fig. 3 Spectrum at the intensity maximum averaged between t = 1.2 s and 2.2 s.

result is the average of the spectra at the intensity maximums between t = 1.2 s and 2.2 s.

Since the observation system is absolutely calibrated, the signals from the detector can be translated into the emitted photon number. Each Balmer series line is fitted with a Gaussian profile and the line intensity $I(p, q)$ [photons s^{-1} m^{-2}], where p and q stand for the principal quantum number of the upper and lower levels, respectively, is determined.

From the viewpoint of atomic processes, the line intensity $I(p, q)$ is understood as

$$I(p, q) = N(p) A(p, q), \tag{6}$$

where $N(p)$ is the line-integrated population density of level p, and $A(p, q)$ is the spontaneous transition probability. We adopt $A(p, q)$ values of the NIST database [9] and derive $N(p)$ from Eq. (6). In Fig. 4 $N(p)$ normalized by their statistical weight $g(p)$ is plotted with the solid squares as a function of the ionization potential of the level p. In

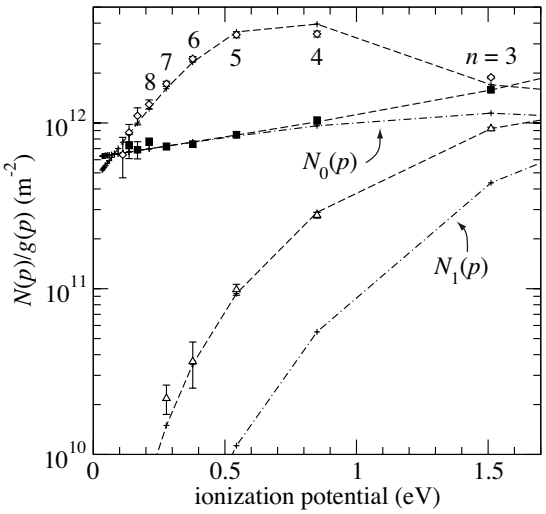

Fig. 4 Population distributions for different three plasma states in the discharge; the solid squares, open circles, and open triangles are obtained for the intensity maximum in the oscillation phase, before the detachment, and in the plasma terminating phase, respectively. Fitting results with the CR model are also shown with the dashed lines. The dotted-dashed lines, which are labeled as $N_0(p)$ and $N_1(p)$ are respectively the recombining plasma component and the ionizing plasma component in the total population $N(p)$ of the ionization balance plasma for the intensity maximum case.

Fig. 4 the results derived for other two different timings are also shown.

We attempt fittings of the all population distributions in Fig. 4 with Eq. (4) by adjusting T_e and n_e. The open triangles in Fig. 4 are taken in the time period from t = 0.6 s to 0.7 s. The population rapidly decreases with the increasing principal quantum number. This behavior is a typical characteristic of the ionizing plasma, for which each level population is dominated by the second term in Eq. (4). Since the dependence of the population distribution on the electron temperature and density is generally weak, it is difficult to uniquely determine those parameters from the obtained population distribution. The dashed line is, for example, the calculation result with T_e = 30 eV and $n_\mathrm{e} = 8 \times 10^{18}$ m^{-3} which is normalized to the measurement.

The open diamonds in Fig. 4 are the result at $t = 2.85$ s in the plasma decay phase after the NBI heating is terminated. The result exhibits a typical characteristic of the recombining plasma; the populations of highly excited levels are relatively large. Roughly speaking, the slope of the highly excited level populations corresponds to T_e and the level having the maximum population to n_e. We fit the result with the first term in Eq. (4) and the parameters of $T_e = 0.2$ eV and $n_e = 1.3 \times 10^{19}$ m^{-3} are obtained. The fitting result is shown with the dashed line in Fig. 4.

The solid squares in Fig. 4 show a different distribution profile from those in the former two cases. No reasonable combination of T_e and n_e is found for the present case when either the pure ionizing plasma or recombining plasma is assumed. Instead, we attempt a fitting under the assumption of the ionization balance plasma. When the ionization rate and the recombination rate are balanced, namely, Eq. (5) is zero, the plasma is defined to be in the ionization balance. The ratio of n_i to $n(1)$ is expressed as

$$\frac{n_i}{n(1)} = \frac{\alpha_{CR}}{S_{CR}}, \tag{7}$$

and Eq. (4) is rewritten as

$$n(p) = \left\{ R_0(p) + R_1(p)\frac{S_{CR}}{\alpha_{CR}} \right\} n_e n_i. \tag{8}$$

The measured population distribution is well fitted with $T_e = 1.8$ eV and $n_e = 2 \times 10^{20}$ m^{-3}. The fitting result normalized to the measurement is shown with the dashed line in Fig. 4. The dotted-dashed lines labeled as $N_0(p)$ and $N_1(p)$ correspond to the first and second terms in Eq. (4). Equation (8) is evaluated with these parameters and $n(3)/g(3) = 7.3 \times 10^{12}$ m^{-3} is obtained. On the other hand, the line-integrated population $N(3)/g(3)$ is determined to be 1.6×10^{12} m^{-2} in the measurement. The normalization factor between these quantities, $\ell = 0.22$ m, corresponds to the thickness of the radiation belt. This result is consistent with that of the AXUVD measurement.

It is surprising that the strong radiation area having such a low electron temperature is located inside the last closed flux surface (LCFS), while the central T_i line is kept at approximately 800 eV. No reasonable explanation has been found to understand the fact that such an extremely low temperature plasma steadily exists in the confinement region of a high temperature plasma.

5 Discussion

The electron temperature and density are determined mainly from the population distribution over the $n = 3$ to $n = 6$ levels, and the points corresponding to $n = 7$ and higher levels apparently deviate from the expected values as seen in Fig. 4. Since the wavelength resolution to measure their corresponding emission lines is insufficient, the uncertainty of the obtained line intensity is large. In order to make clear this uncertainness, a measurement with higher wavelength resolution has been attempted for a similar discharge. The spectrum measured with the same spectrometer but with a grating of 1800 grooves/mm is shown in Fig. 5. The synthetic spectrum with the same plasma parameters as derived in the analysis above, i.e., $T_e = 1.8$ eV and $n_e = 2 \times 10^{20}$ m^{-3}, is also shown in the same figure. Here, the Stark broadening for individual line profiles is calculated with the numerical calculation data [11]. The agreement is satisfactory in both the intensity distribution and line profiles, and the plasma parameters derived here are verified.

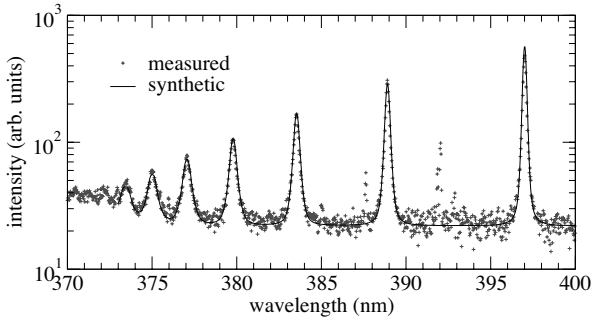

Fig. 5 Spectrum at the intensity maximum with a high wavelength resolution measurement. The solid line is a synthetic spectrum calculated with $T_e = 1.8$ eV and $n_e = 2 \times 10^{20}$ m^{-3} and normalized to the measurement. The Stark broadening and the instrumental width are taken into account for each line profile.

Acknowledgments

The authors are grateful to the LHD experimental group for the helpful support. This study has been made in part under a financial support by the LHD project (NIFS07ULPP527).

[1] J. Neuhauser, M. Alexander, G. Becker, et al., Plasma Phys. Control. Fusion **37**, A37 (1995).
[2] C. S. Pitcher and P. C. Stangeby, Plasma Phys. Control. Fusion **39**, 779 (1997).
[3] A. Loarte, R. D. Monk, J. R. Martín-Solís, et al., Nucl. Fusion **38**, 331 (1998).
[4] N. Asakura, S. Sakurai, H. Tamai, et al., J. Nucl. Mater. **290–293**, 825 (2001).
[5] U. Wenzel, K. McCormick, N. Ramasubramanian, et al., Nucl. Fusion **44**, 1130 (2004).
[6] J. Miyazawa, S. Masuzaki, R. Sakamoto, et al., Nucl. Fusion **46**, 532 (2006).
[7] S. Masuzaki, R. Sakamoto, J. Miyazawa, et al., J. Plasma Fusion Res. **81**, 649 (2005).
[8] B. J. Peterson, A. Yu. Kostrioukov, N. Ashikawa, et al., Plasma Phys. Control. Fusion **45**, 1167 (2003).
[9] NIST Atomic Spectra Database http://physics.nist.gov/PhysRefData/ASD/index.html)
[10] T. Fujimoto, S. Miyachi, and K. Sawada, Nucl. Fusion **28**, 1255 (1988).
[11] C. Stehlé and R. Hutcheon, Astron. Astrophys. Suppl. Ser. **140**, 93 (1999).